Breakup of cw multimode oscillations and low-frequency instability in a microchip solid-state laser by high-density pumping

Kenju Otsuka
Department of Applied Physics, Tokai University, 1117 Kitakaname, Hiratsuka, Kanagawa, 259-12 Japan

Paul Mandel
Optique Nonlinéaire Théorique, Université Libre de Bruxelles, Campus Plaine Code Postal 231, 1050 Bruxelles, Belgium

E. A. Viktorov
Institute for Laser Physics, 199034 St. Petersburg, Russia
(Received 12 May 1997)

The effect of high-density pumping on lasing mode spectra is investigated in a laser-diode pumped microchip $LiNdP_4O_{12}$ (LNP) laser. Breakup of multimode oscillations, leading to single-mode oscillations, is observed experimentally. It is shown analytically that the enhanced Auger recombination process among excited Nd ion pairs results in a strong deformation of spatial hole-burning patterns, leading to a destabilization of the multimode laser output via a quadratic-to-quartic transition of the spatial distribution of population inversion. The destabilization threshold is shown to be given by a universal relation which reproduces experimental results quite well. A mode-partition instability is observed above the transition, whose properties are intimately related to the antiphase dynamics. [S1050-2947(97)03610-X]

PACS number(s): 42.50.−p, 42.55.Rz

I. INTRODUCTION

The spatial hole-burning effect of population inversion resulting from lasing standing-wave patterns in Fabry-Perot laser resonators was introduced by Tang, Statz, and deMars (TSD) in the early 60's [1]. It is the fundamental physical process which allows multimode oscillations in homogeneously broadened solid-state lasers. This is due to the slow spatial diffusion of population inversions in solid-state laser crystals such as YAG. TSD expanded the distribution of population inversion into spatial Fourier components and derived the so-called TSD equations by retaining only the space average and Fourier components varying at optical wave numbers [1]. The relation between lasing mode number and pump rate was deduced from the TSD equations [1,2] and was verified experimentally in various solid-state lasers including Nd:YAG lasers [3].

The recent rapid progress of high-power laser-diode pumped microchip lasers has driven a renaissance of solid-state laser physics research and led to novel phenomena, such as winner-takes-all dynamics and antiphase periodic states [4,5], antiphase dynamics [6–8], dynamical nonreciprocal independence [9], and universal power spectra relation in multimode lasers [10,11]. One of the most peculiar features inherent in high-power laser-diode pumped miniature microchip solid-state lasers is the Auger recombination process among excited ions, which is expected in microchip lasers with high-density pumping [12]. In the Auger process, two excited electrons in the $^4F_{3/2}$ level interact due to excited state absorption: one electron makes a transition to the lower laser level $^4I_{11/2}$ emitting a 1.05 μm photon, while another electron is excited to the higher energy level $^2GI_{9/2}$. The Auger coefficient is proportional to excited ion density N_e and a strong Auger effect is expected in state-of-art high-power laser-diode-pumped microchip lasers with high-density pumping such as Nd:YVO, Nd:LSB, Cr:LiSAF, etc. Particularly, Nd stoichiometric (e.g., direct compound) lasers such as NdP_5O_{14} [13], $LiNdP_4O_{12}$ [14], $NdAl_3(BO_3)O_4$ [15], and Nd:$CeCl_3$ [16] developed in the early 70's in which the Nd ion concentration is 30 times higher than in conventional microchip lasers, are promising candidates for investigating the effect of Auger recombination process on spatial hole-burning and multimode oscillations.

In this paper, the effect of high-density pumping on spatial hole-burning is investigated experimentally and theoretically. In Sec. II, experimental results concerning the effect of high-density pumping on lasing mode spectra are shown by using a laser-diode pumped microchip LNP laser. It is shown that the breakup of multimode oscillations, leading to single-mode oscillation, takes place above a critical pump density threshold. In Sec. III, analytical results on the high-density pumping effect are described and it is shown that the Auger recombination process inhibits the multimode regime in favor of the single mode regime. A simple criterion is derived for the critical pump power at which the multimode operation becomes unstable. These theoretical results are shown to reproduce experimental results quite well. In Sec. IV, an instability associated with the deformation of the spatial distribution of population inversion is demonstrated experimentally.

II. EXPERIMENTAL RESULTS

A. Input-output characteristics

Experiments were carried out by using a laser diode (LD)-pumped LNP laser. An experimental setup of an LD-pumped microchip LNP laser is depicted in Fig. 1. The LNP crystal was 1-mm thick and dielectric mirrors were coated on both

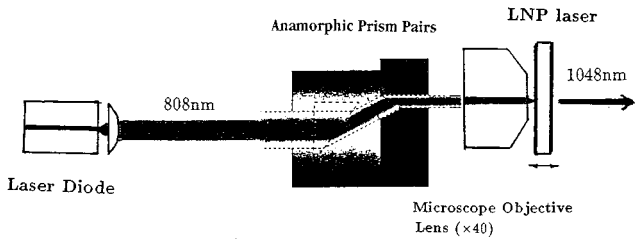

FIG. 1. Experimental apparatus of a laser-diode pumped LNP laser.

ends of the crystal. The output coupling was 1% at 1048 nm. A collimated lasing beam from the laser diode oscillating at $\lambda_p = 808$ nm was passed through anamorphic prism pairs to transform an elliptical beam into a circular beam and was focused onto the LNP crystal by a microscope objective lens (M 40×). By changing the distance between the lens and the LNP crystal, the pump beam spot size was controlled. A linearly-polarized TEM_{00} mode oscillation along the pseudoorthorohmbic b axis was observed.

Input-output characteristics measured for different pump spot sizes are shown in Fig. 2. Here, the effective pump beam spot size w_p averaged over the absorption length $l_p \simeq 1/\alpha_p = 100$ μm ($\alpha_p \simeq 100$ cm^{-1} is the absorption coefficient of LNP at $\lambda_p = 808$ nm) was estimated to be 50 μm (a), 40 μm (b), and 25 μm (c) from the pumped cross section, respectively. Such a short absorption length implies that the population inversion is strongly localized at the input mirror region inside the laser resonator. The number of oscillating modes is added in the figures. The oscillating beam spot size was estimated to be $w_0 \simeq 150$ μm and the slope efficiency is found to increase as the pump spot size w_p is decreased.

In the case of Fig. 2(a), we find from the measured threshold pump power that $N_e/N_0 = N_{\rm th}/N_0 \simeq 0.028$, where $N_{\rm th}$ is the threshold Nd density for lasing, N_e is the excited Nd density, and N_0 is the Nd concentration in LNP crystals [14]. In this case, usual input-output characteristics, in which the number of oscillating modes increases with the pump power [1–3], are obtained. When the pump power density is increased by decreasing the pump beam spot size, unusual input-output characteristics are observed as shown in Fig. 2(b). In the case of Fig. 2(b), $N_e/N_0 \simeq 0.046$ and the breakup of multimode oscillation is found to occur at $w \equiv P/P_{\rm th} = w_c \simeq 2$ indicated by an arrow, at which a number of modes begins to decrease, leading to single-mode oscillation, where P is the pump power and $P_{\rm th}$ is the threshold pump power. As the pump power density is increased further as in Fig. 2(c), spontaneous single-mode oscillation is observed in the entire pumping domain. In the case of Fig. 2(c), the extremely high-density pumping of $N_e/N_0 \simeq 0.1$ is attained. In fact, in LNP crystals, each Nd ion has eight nearest-neighbor Nd ions [17]. Therefore, in the case of Fig. 2(c), an excited ion will, on average, begin to see one excited ion among its nearest neighbors, assuming $N_0 = 4.37 \times 10^{21}$ cm^{-3} [14].

Observed spontaneous single-mode oscillations are very attractive from the view point of practical applications. In particular, single-mode oscillations in a 1-mm-thick LNP laser ensures laser-diode pumped single-frequency intracavity second-harmonic generations (ISHG) by attaching a frequency-doubling crystal to the LNP crystal. The single-mode oscillation in ISHG enables us to avoid instabilities (e.g., ''green problem'') resulting from ISHG in multimode lasers [18].

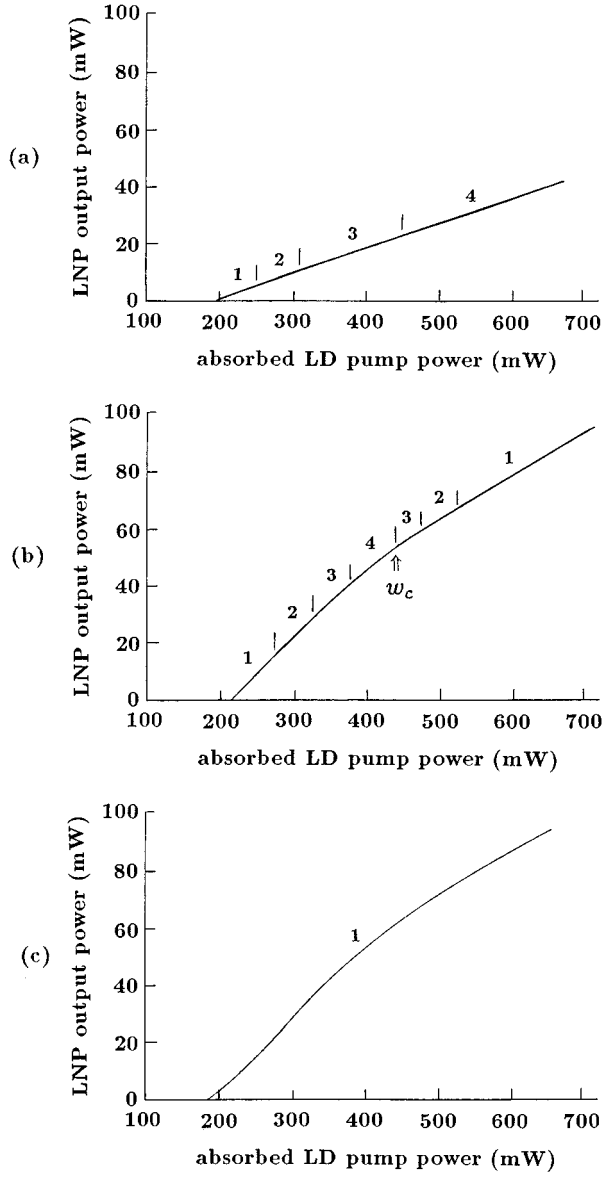

FIG. 2. Input-output characteristics and number of oscillating modes in a laser-diode-pumped LNP laser for different pump densities.

B. Antiphase relaxation oscillations

In the case of multimode class-B lasers with spatial hole burning, in which polarization lifetime is much shorter than the population inversion lifetime τ, it has been established from intensive theoretical and experimental studies that the total output features damped relaxation oscillations at a unique frequency $f_1 = (1/2\pi)\sqrt{(w-1)/\tau\tau_p}$ (τ_p: photon lifetime), while each mode exhibits N relaxation oscillations, namely, $f_1 > f_2 > \cdots > f_N$, where N is the number of lasing modes [6–8]. The so-called McCumber frequency f_1 corresponds to the relaxation oscillation frequency in a single mode laser derived from the simple linear stability analysis of a single-mode laser. In other terms, individual modes are

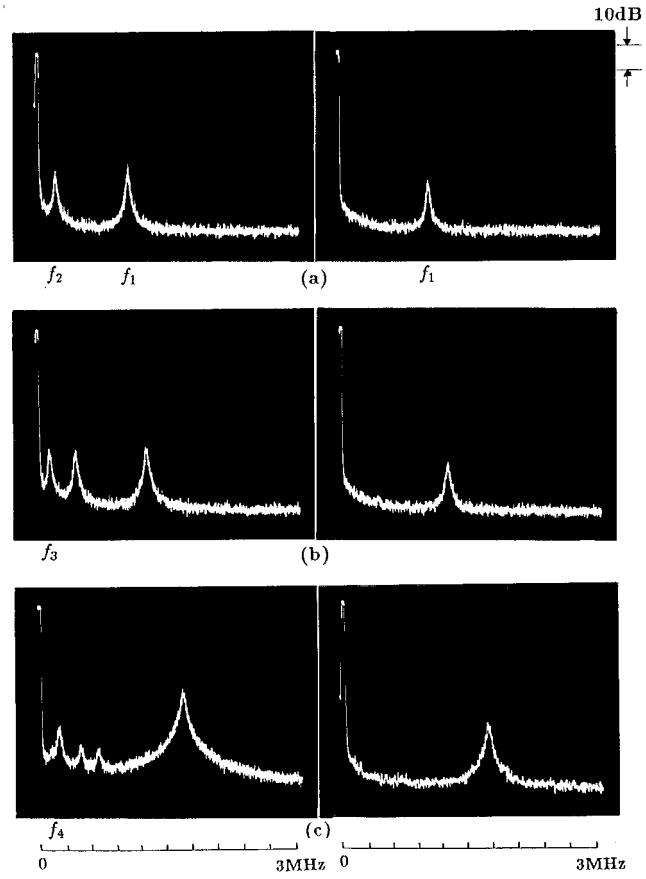

FIG. 3. Power spectra for modal and total outputs in the free-running LNP laser corresponding to Fig. 2(b). (a) Two-mode regime, (b) three-mode regime, and (c) four-mode regime. Left-hand figures indicate power spectra of the first-lasing mode and right-hand figures indicate power spectra for the total output. For the total output, input power to rf spectrum analyzer was attenuated by -10 dB. vertical scale: 10 dB/div. horizontal scale: 300 kHz/div.

self-organized to exhibit antiphase dynamics such that low frequency relaxation oscillations are strongly suppressed in the total output.

In the present experiment, such self-organized nature concerning antiphase relaxation oscillations was confirmed in multimode oscillation regimes independently of the pump power density. Examples are shown in Fig. 3, where measurements were carried out in multimode regimes below the critical pump w_c in Fig. 2(b). The left-hand photographs correspond to power spectra for the first lasing mode at the wavelength $\lambda_{l,1}=1047.6$ nm, which corresponds to the ${}^4F_{3/2}(1)\rightarrow{}^4I_{11/2}(1)$ transition, and the right-hand photographs correspond to power spectra for the total output. It is apparent that relaxation oscillation peaks are strongly suppressed in the total output, except at the McCumber frequency f_1 which are driven by ''white'' noise. We shall refer to this property later on in this paper as generic antiphase property. In Fig. 3, the second lasing mode appears via the ${}^4F_{3/2}(1)\rightarrow{}^4I_{11/2}(2)$ transition at $\lambda_{l,2}=1055$ nm, the third lasing mode appears via the ${}^4F_{3/2}(1)\rightarrow{}^4I_{11/2}(3)$ transition at $\lambda_{l,3}=1060$ nm, and the fourth lasing mode appears at $\lambda_{l,4}=1048$ nm which belongs to the ${}^4F_{3/2}(1)\rightarrow{}^4I_{11/2}(1)$ transition. Note that the longitudinal mode spacing is an order of magnitude larger than the value determined by the cavity length L, which gives $\Delta\lambda=\lambda^2/2nL=0.34$ nm. On the contrary, above the critical pump w_c, the 1048 nm mode stops lasing at first as the pump power is increased, the 1047.6 nm mode is turned off next, and then the 1055 nm mode is turned off, and finally single-mode oscillation at 1060 nm survives. Similar multiple-transition oscillations featuring ''cross mode'' (see Fig. 10(c) of [19]) was reported in Ar laser pumped LNP lasers reflecting the decrease in reabsorption loss in unpumped region of the LNP crystal, $L_{\rm ra}(1.048)>L_{\rm ra}(1.055)>L_{\rm ra}(1.060)$ [19]. Each of these transitions supports the lasing of many longitudinal modes separated by $\Delta\lambda$. In the present case, due to the strong localization of the population inversion near the input mirror, nearby modes separated by $\Delta\lambda$ are strongly quenched as a result of the mode competition through the strong cross saturation [20]. Generic antiphase relaxation oscillation property was observed both below and above the critical pump. From these observations, it is concluded that antiphase dynamics inherent in multimode lasers with spatial hole burning holds even in the case of multiple-transition oscillations by high-density pumping.

C. Ar laser and Kr laser pumping

Experimental results described so far strongly implies that high-density pumping results in unusual input-output characteristics. To verify this idea more precisely, we employed other pump sources with different absorption coefficients α_p instead of the laser diode, to change pump power density more drastically. For this purpose, an Ar laser ($\lambda_p=5145$ Å, $\alpha_p=23\ {\rm cm}^{-1}$) or a Kr laser ($\lambda_p=7993$ Å, $\alpha_p=250\ {\rm cm}^{-1}$) served as a pump. The absorption lengths $l_p\simeq\alpha_p^{-1}$ were 435 μm for 5145 Å and 40 μm for 7993 Å, respectively.

In the case of Ar laser pumping, in which absorption length is much longer than LD pumping, usual multimode oscillation characteristics such as in Fig. 2(a) were observed for various pump beam spot sizes. For Kr laser pumping, in which the pump wavelength matches with the absorption peak of LNP crystals [21], spontaneous single-mode oscillations were observed in entire pump regimes.

III. THEORETICAL RESULTS

A. Smoothing effects of spatial hole-burning pattern

The favored single-mode oscillations in high pump density regimes [e.g., Figs. 2(b) and 2(c)], strongly suggest that spatial hole burning patterns tend to be smeared out as the pump power density is increased. A first source of smoothing of spatial hole burning pattern is resonant transfer, i.e., reabsorption process [21], as shown in Fig. 4(a). Since the relaxation energy is transferred in full to one of the neighbor *nonexcited* ions, all fluorescence transitions can contribute to resonance transfer. This is effective since the overlapping between emission and absorption lines is perfect. Especially, the ${}^4I_{9/2}(1)\rightarrow{}^4F_{3/2}(1)$ transition from the ground state is the most effective in resonance transfer for LNP crystals. Based on the spectroscopic data of LNP [21], the transfer probability of excitation energy to one of the neighbor ions via the ${}^4I_{9/2}\rightarrow{}^4F_{3/2}$ reabsorption process is estimated to be W_J

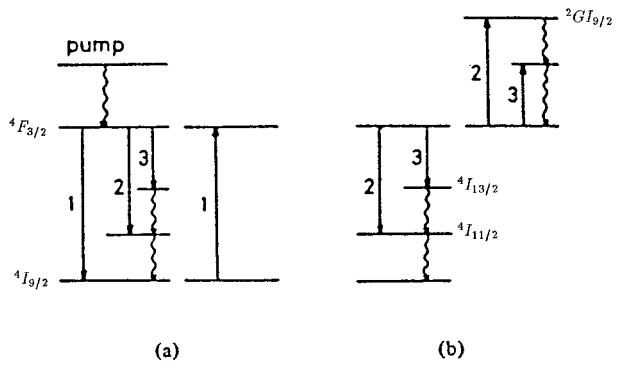

FIG. 4. Models of (a) fluorescence reabsorption process and (b) Auger recombination process in LNP lasers. Here, 1 indicates the transition between the ground state and the excited state at 870 nm, 2 corresponds to the lasing transition at 1048 nm for ↓ and corresponding excited state absorption for ↑, 3 corresponds to the lasing transition at 1320 nm for ↓ and corresponding excited state absorption for ↑.

$=1.2\times10^8$ s^{-1}, which yields the diffusion distance $d\sqrt{W_J\tau}$ $=800$ Å in LNP crystals, where $d=6$ Å is the mean separation between Nd ions and $\tau=120$ μs. Since this is much shorter than a quarter-wave length, spatial hole-burning pattern is not sufficiently smeared out by this energy migration process in LNP crystals.

The second possible mechanism is Auger recombination process depicted in Fig. 4(b), in which two *excited* Nd ions interact and the pair annihilation takes place through excited state absorption via the $^4F_{3/2}\rightarrow{}^2GI_{9/2}$ transition in LNP crystals. Since this process occurs in proportion to N_e^2, the enhanced deformation of spatial hole-burning pattern is expected in high pump density regimes. In the following, the effect of Auger recombination process on spatial hole burning pattern is analyzed theoretically.

B. Quadratic-to-quartic transition of spatial hole-burning pattern

The rate equation for the population inversion density $N(z)$ including Auger recombination process is given by

$$\frac{dN(z)}{dt}=P(z)-\frac{[1+q_2N(z)]N(z)}{\tau}-B_cN(z)S(z), \quad (1)$$

where $P(z)$ is the pump rate, τ is the population lifetime, q_2 is the Auger parameter, B_c is the stimulated emission coefficient, and $S(z)$ is the photon density. Let us introduce the population inversion density at the lasing threshold averaged over the absorption length $N_{\rm th}=(1/l_p)\int_0^{l_p}N(z)dz$. For the LNP laser, $l_p\simeq100$ μm. Defining a normalized population inversion through $n(z,t)\equiv N(z,t)/N_{\rm th}$, we find in steady state

$$n(z)=\frac{-1-s(z)+\sqrt{[1+s(z)]^2+4q_2N_{\rm th}(z)w(z)}}{2Q_2}. \quad (2)$$

Here, $w=\tau P/N_{\rm th}$ is the normalized pump power, $s(z)$ $=B_cS(z)\tau$ is the normalized photon density, and Q_2 $\equiv q_2N_{\rm th}$ is the normalized Auger parameter. Assuming $4q_2N_{\rm th}w\ll[1+s(z)]^2$ and $s(z)=s_1\sin^2k_1z$, where k_1 and s_1 are, respectively, the wave number and the photon density of the first lasing mode, Eq. (2) is approximated by

$$n(z)\simeq\frac{w}{1+s_1\sin^2kz}-\frac{Q_2w^2}{[1+s_1\sin^2kz]^3}, \quad (3)$$

where we have also assumed $w=(1/l_p)\int_0^{l_p}w(z)dz$. In NdP_5O_{14} lasers, for example, $Q_2=1.8$ when the excited Nd ion density N_e is 50% of the total Nd ion concentration N_0 [12]. Equation (3) expresses the population inversion distribution when only the first lasing mode is oscillating.

If Q_2 is sufficiently small, the function $n(z)$ has two maxima and two minima in a period $0\leqslant kz<2\pi$. If Q_2 is sufficiently large, the function $n(z)$ has four maxima and four minima in each period. At the transition between these two domains, two extrema of $n(z)$ coincide which means that $n(z)$ has quartic instead of quadratic extrema. Expanding $n(z)$ around its maximum $n(z)=n(z_{\rm max})+(z-z_{\rm max})^2n''$ $+\cdots$, the quadratic-to-quartic (Q2Q) transition is characterized by $n''=0$. Solving this equation for the critical pump at which this transition occurs yields the relation

$$w_c=\frac{1}{3Q_2}. \quad (4)$$

This simple *universal relation* implies that *the transition occurs independently of the first lasing mode intensity s_1 and that the critical pump is determined only by the Auger parameter*.

A numerical example based on Eq. (3) is given in Fig. 5. Here, $Q_2=0.1$, 0.17 and 0.36 are assumed, where these values correspond to the estimated Q_2 values for Figs. 2(a), 2(b), and 2(c), respectively. For moderate values of Q_2, as in Fig. 5(a), the quadratic-to-quartic transition is not reached for reasonable values of the pump rate. For larger Q_2, the transition is reached for finite pumping ($w_c\simeq2$ for Q_2 $=0.17$) and the population inversion distribution is strongly deformed above w_c as shown in Fig. 5(b). The w_c-value agrees with the analytic result obtained from Eq. (4) as well as with the observed value in Fig. 2(b). Consequently, the overlap integral between empty cavity eigenmodes and the deformed population inversion pattern is decreased as the pump is increased in the regime above w_c. Eventually, multimode oscillations becomes unstable. This result parallels the change of slope observed around w_c in Fig. 2(b). At the critical pump $w=w_c$, the population distribution displays the plateau characteristic of the quartic maximum as shown in Fig. 5(b). Finally, in the case $Q_2\geqslant1/3$, shown in Fig. 5(c), the standing-wave pattern is no more sinusoidal right from the lasing threshold, leading to spontaneous single-mode oscillation. In other terms, the dip in the center of $n(z)$ corresponds to the node of the eigenfunctions, whereas side dips cut excess energy in antinodes.

Although the condition given by Eq. (4) was derived in the single mode regime, we have verified numerically that it still gives a good approximation of w_c in the multimode regime in the range of pump rate used in the experiments, in which a number of modes is not large.

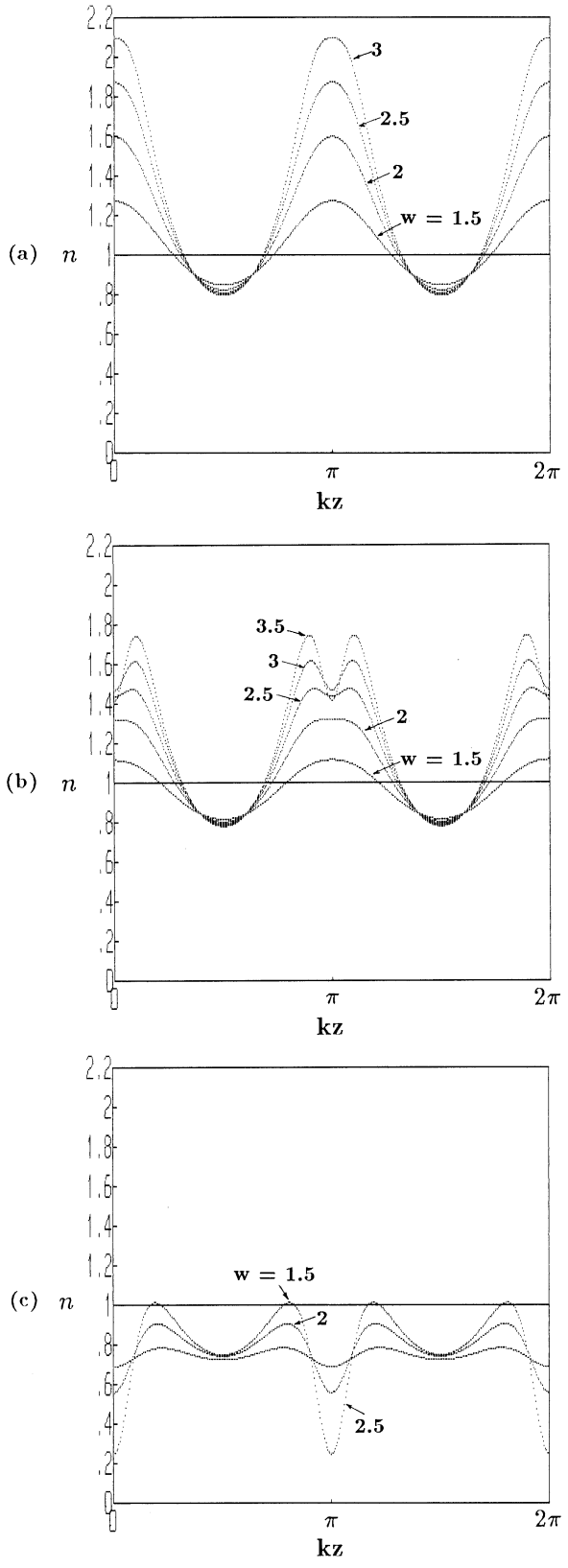

FIG. 5. Numerical spatial distribution of population inversion for various pump levels when the first lasing mode is oscillating. (a) $Q_2=0.1$, (b) $Q_2=0.17$, (c) $Q_2=0.36$. The first lasing mode intensity was assumed to be $s_1=(\frac{4}{3})(w-1)$, which is easily derived from simple calculations. In case (b), the quadratic-to-quartic transition occurs at $w=w_c\simeq 2$.

IV. INSTABILITY ASSOCIATED WITH DEFORMATION OF SPATIAL HOLE-BURNING PATTERN

A. Mode-partition noise above the Q2Q transition

When the pump is increased beyond w_c, a *mode-partition* instability appears in the multimode domain above w_c, before the single mode domain is reached. The threshold pump for the onset of this instability depends on the pump condition (spot size). A typical example of oscillation wave forms and corresponding power spectra for modal outputs is shown in Fig. 6 in the three-mode regime. The power spectrum exhibits a peculiar spectrum around $f_{Mp}\simeq 1.3$ MHz, which is indicated by the arrow ⇑. It consists of many closely spaced line spectra separated by $f_{mp}\simeq 1$ kHz, in addition to relaxation oscillation frequency peaks f_1, f_2, f_3 driven by white noise, as is shown in Fig. 6(b). The corresponding modal output wave form in Fig. 6(a) shows fluctuation roughly at 1 kHz. The amplitude of fluctuation was measured to be about 10% of the averaged output power.

This fluctuation component shifts towards a higher frequency side as the pump power is increased. Results are shown in Fig. 7, where two-mode oscillation is occurring. In this case, the power spectrum for the modal output features additional large amplitude broad-band fluctuation components peaked around 100 kHz indicated by the arrow ↑ in Fig. 7(b), in addition to the relaxation oscillation frequency peaks at f_1 and f_2. The corresponding wave form in an expanded time scale features random fluctuation at 100 kHz as shown in Fig. 7(a). This tendency of the appearance of broad-band noise was always observed when the pump power density was increased.

It should be noted that this instability occurring above the quadratic-to-quartic transition disappears completely for the total output. This is shown in Figs. 6(c) and 7(c), in which only the McCumber frequency peak f_1 is observed. Thus, the modal outputs exhibit anticorrelated amplitude fluctuations, while the total output is completely free from such mode-partition instability. The strong suppression of low-frequency relaxation oscillations at f_2 and f_3 for the total output results from the usual antiphase dynamics mentioned in Sec. II [6–8]. However, the classic TSD multimode rate equations are unable to describe the mode-partition instability reported in this section.

B. Discussion

The mode-partition instability reported in this section was not observed in the case of Fig. 2(c), in which spontaneous single-mode oscillation is ensured as shown in Fig. 5(c). This strongly implies that multimode oscillations above the transition derived from Eq. (4) is the key for understanding this instability. We introduced such effects as the higher-order spatial Fourier components of spatial hole-burning pattern and the strong localization of population inversion at the input end surface of the crystal, in addition to the Auger recombination effects, into TSD multimode equations. These effects are found to increase the second lasing mode threshold further. In addition, the breakup of multimode oscillations featuring the decrease in mode numbers 4→3→2→1 observed in the experiment has been reproduced. However,

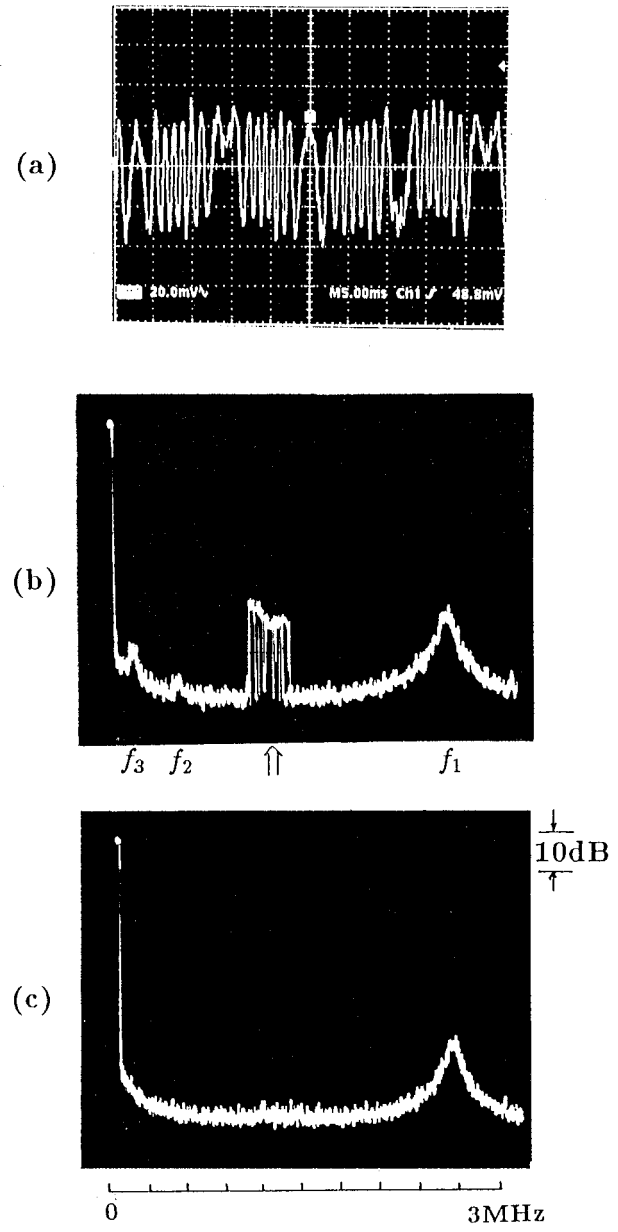

FIG. 6. (a) Modal output wave form, (b) corresponding power spectrum, and (c) power spectrum for the total output indicating mode-partition instability featuring antiphase dynamic properties. The pump power was set in the three-mode oscillation domain above the kink w_c. (a) horizontal scale: 5 ms/div. (b),(c) horizontal scale: 300 kHz/div. vertical scale: 10 dB/div. For the total output spectrum, the input signal was attenuated by -10 dB. The disappearance of f_2 and f_3 peaks result from usual antiphase dynamics.

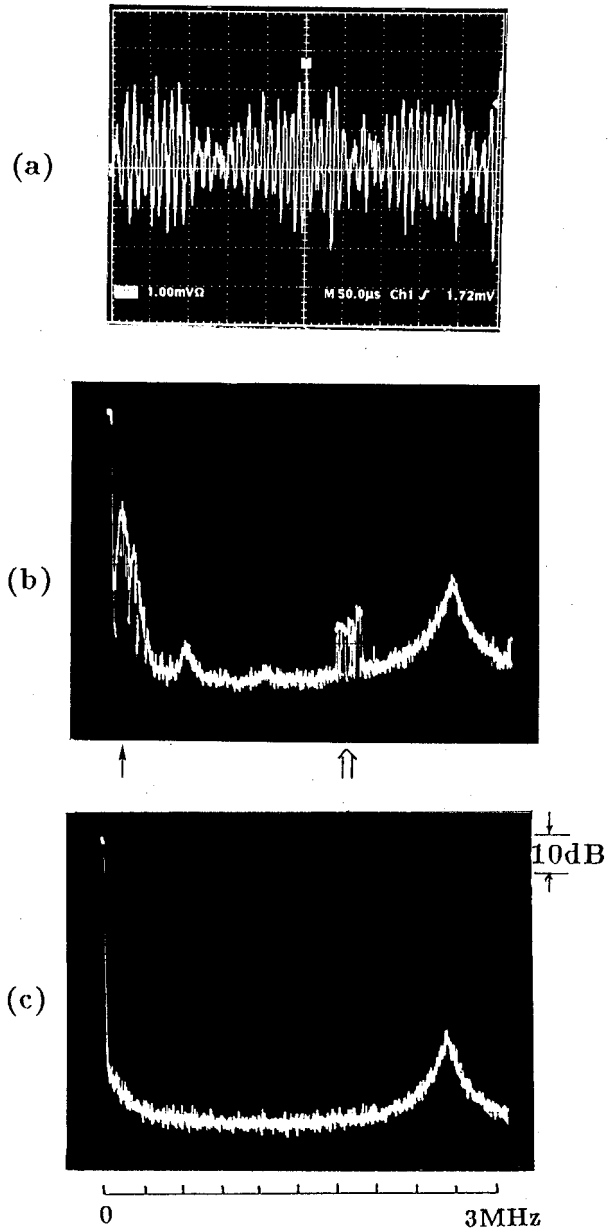

FIG. 7. Mode-partition instability observed when the pump power was increased. (a) Modal output wave form in an expanded time scale of 50 μs/div. (b) Power spectrum: 300 kHz/div. All the fluctuation components except for f_1 were also suppressed for the total output.

solutions of eigenvalue problem (e.g., linear stability analysis) of these modified TDS equations tell us that no instability appears.

These results suggest that in these high-density pumping regimes, there is no longer a one-to-one correspondence between cavity modes and lasing modes. In other terms, we must investigate spatiotemporal multimode laser dynamics including a large number of cavity modes and a spatial distribution of population inversion in the beam propagation direction. The observed instability will be best described by equations in which modal expansions have not yet been introduced. Another peculiar feature to be bear in mind is the interplay between lasing modes belonging to different transitions. Here, the wavelength separation of these modes $\Delta\lambda_L \simeq 5$ nm is of the same order of magnitude as the fluorescence linewidth of each transition $\Delta\lambda_F \propto T_2$, the transverse relaxation time [21].

A feature of this problem is the Auger effect which leads to a high-density correction proportional to N^2 in the evolution of the population inversion. In view of the modal expansion which leads to the usual TSD equations, the N^2 term will induce a second source of recurrence: each modal amplitude $D(n;q,t)=(1/L)\int_0^L D^n(z,t)\cos(2\pi qz/L)dz$ will depend on $D(n;q\pm q',t)$ as in the TSD equations but also on

$D(n+1;q,t)$. Hence a new truncation scheme is necessary to account for the Auger effect. Work along this direction is in progress and will be reported in a separate publication.

V. CONCLUSION

In conclusion, the breakup of multimode oscillations in a laser-diode pumped microchip stoichimetric $LiNdP_4O_{12}$ laser due to the strong deformation of spatial hole-burning patterns, which arises from high-density pumping, has been investigated. A simple universal relation between critical pump and Auger parameter for quadratic-to-quartic transition of population distribution function, which supports the experimental results on lasing mode spectra, has been given. Spontaneous single-mode oscillation has been realized according to this relation.

A mode-partition instability has been found to occur, which is associated with the strong deformation of population inversion distribution above the quadratic-to-quartic transition, and its challenging property has been shown experimentally. A full theoretical explanation of this instability is now under investigations. However, the present low-frequency instability provides research issues for laser physics involving multimode laser dynamics.

ACKNOWLEDGMENTS

K.O. is indebted to T. Yamada of NTT Basic Research Laboratories for supplying the LNP crystals. The work in Tokai University was supported by Grant-in-Aid for Scientific Research of The Ministry of Education. The work in Brussels was supported by the Fonds National de la Recherche Scientifique, the Interuniversity Attraction Pole program of the Belgian government, and a grant from the Services Fédéraux des Affaires Scientifiques, Techniques et Culturelles.

[1] C. L. Tang, H. Statz, and G. deMars, J. Appl. Phys. **34**, 2289 (1963).
[2] H. Statz and C. L. Tang, J. Appl. Phys. **35**, 1377 (1964).
[3] T. Kimura, K. Otsuka, and M. Saruwatari, IEEE J. Quantum Electron. **QE-7**, 225 (1971).
[4] K. Wiesenfeld, C. Bracikowski, G. James, and R. Roy, Phys. Rev. Lett. **65**, 1749 (1990).
[5] K. Otsuka, Phys. Rev. Lett. **67**, 1090 (1991).
[6] K. Otsuka, P. Mandel, S. Bielawski, D. Derozier, and P. Glorieux, Phys. Rev. A **46**, 1692 (1992).
[7] P. Mandel, M. Georgiou, K. Otsuka, and D. Pieroux, Opt. Commun. **100**, 341 (1993).
[8] K. Otsuka, Proc. SPIE **2039**, 182 (1993), and references therein.
[9] P. Mandel and J.-Y. Wang, Opt. Lett. **19**, 533 (1994).
[10] P. Mandel and J.-Y. Wang, Phys. Rev. Lett. **75**, 1923 (1995).
[11] P. Mandel, K. Otsuka, J.-Y. Wang, and D. Pieroux, Phys. Rev. Lett. **76**, 2694 (1996).
[12] M. Blätte, H. G. Danielmeyer, and R. Ulrich, Appl. Phys. **1**, 275 (1980).
[13] H. G. Danielmeyer and H. P. Weber, IEEE J. Quantum Electron. **QE-8**, 805 (1972).
[14] T. Yamada, K. Otsuka, and J. Nakano, J. Appl. Phys. **45**, 5096 (1974).
[15] S. R. Chinn and H. Y.-P. Hong, Opt. Commun. **15**, 345 (1975).
[16] S. Singh, R. B. Chester, W. H. Brodkiewics, J. R. Potopowics, and L. G. Van Uitert, J. Appl. Phys. **46**, 436 (1975).
[17] H. Koizumi, Acta Crystallogr. Sect. B **32**, 266 (1976).
[18] T. Baer, J. Opt. Soc. Am. B **3**, 1175 (1986).
[19] K. Otsuka, IEEE J. Quantum Electron. **QE-14**, 1007 (1979); K. Otsuka and T. Yamada, Opt. Commun. **17**, 24 (1976).
[20] W. E. Lamb, Jr., Phys. Rev. **134**, A1429 (1964).
[21] K. Otsuka, T. Yamada, M. Saruwatari, and T. Kimura, IEEE J. Quantum Electron. **QE-11**, 330 (1975).